

## Magnetic Properties

**[Cs<sub>6</sub>Cl][Fe<sub>24</sub>Se<sub>26</sub>]: A Host–Guest Compound with Unique Fe–Se Topology**

Martin Valldor,<sup>\*[a]</sup> Bodo Böhme,<sup>[a]</sup> Yurii Prots,<sup>[a]</sup> Horst Borrmann,<sup>[a]</sup> Peter Adler,<sup>[a]</sup> Walter Schnelle,<sup>[a]</sup> Yves Watier,<sup>[b]</sup> Chang Yang Kuo,<sup>[a]</sup> Tun-Wen Pi,<sup>[c]</sup> Zhiwei Hu,<sup>[a]</sup> Claudia Felser,<sup>[a]</sup> and Liu Hao Tjeng<sup>[a]</sup>

**Abstract:** The novel host–guest compound [Cs<sub>6</sub>Cl][Fe<sub>24</sub>Se<sub>26</sub>] (*I4/mmm*; *a* = 11.0991(9), *c* = 22.143(2) Å) was obtained by reacting Cs<sub>2</sub>Se, CsCl, Fe, and Se in closed ampoules. This is the first member of a family of compounds with unique Fe–Se topology, which consists of edge-sharing, extended fused cubane [Fe<sub>8</sub>Se<sub>6</sub>Se<sub>8/3</sub>] blocks that host a guest complex ion, [Cs<sub>6</sub>Cl]<sup>5+</sup>. Thus Fe is tetrahedrally coordinated and divalent

with strong exchange couplings, which results in an ordered antiferromagnetic state below *T<sub>N</sub>* = 221 K. At low temperatures, a distribution of hyperfine fields in the Mössbauer spectra suggests a structural distortion or a complex spin structure. With its strong Fe–Se covalency, the compound is close to electronic itinerancy and is, therefore, prone to exhibit tunable properties.

## Introduction

The chemistry of heavier chalcogenides has made a giant leap forward since the discovery of superconductivity in Fe<sub>1+x</sub>Se.<sup>[1]</sup> This binary belongs to a group of emerging compounds with tetrahedral coordination of Fe<sup>2+</sup> by chalcogenides with considerable electronic itinerancy, which leads to interesting physical phenomena: Spin- or charge-density waves observed in Fe<sub>1+x</sub>Se<sup>[2,3]</sup> are discussed as being closely related to the superconductivity that appears at relatively lower temperatures (*T<sub>c</sub>*). Recently, it was discovered that *T<sub>c</sub>* of FeSe can be increased from 8 to 46 K by interleaving monolayers with molecular<sup>[4]</sup> or ionic<sup>[5]</sup> spacers, to form homogeneous interfaces between FeSe and insulators. The latter also falls into the concept of host–guest compounds, in which the layers of FeSe host the polarizable intercalated guest ions and molecules, as was discussed for the mineral tochilinite, which is based on Fe<sub>1–x</sub>S.<sup>[6]</sup> Obviously, new topologies of Fe–Se-based materials have to be further explored, in search of novel interfaces and lattices that are prone to exhibit exotic electronic states.

A few decades ago, the mineral bartonite<sup>[7]</sup> was first discovered and found to have variable composition,<sup>[8]</sup> which was

later revised to K<sub>6–x</sub>Fe<sub>24–y</sub>S<sub>26</sub>(S,Cl)<sub>1–z</sub>.<sup>[9,10]</sup> Bartonite is structurally related to djerfisherite [K<sub>6</sub>Cl][Li][Fe<sub>24</sub>S<sub>26</sub>]<sup>[11]</sup> and pentlandite (Ni,Fe)<sub>9</sub>S<sub>8</sub><sup>[12]</sup> through a common fused-cubane building block, [Fe<sub>8</sub>S<sub>6</sub>]. The close relation between this fused-cubane cluster and the active site in the enzyme nitrogenase, which catalyzes the essential nitrogen fixation reaction in nature,<sup>[13,14]</sup> was already realized by Pohl and Opitz.<sup>[15]</sup> Strong electron correlations dominate in these iron sulfide-based systems, for example, the minerals are insulators as indicated by their yellow-brown color.<sup>[9,10]</sup> To enhance the chance of electronic itinerancy in such fused-cubane-based structures, S<sup>2–</sup> can be replaced with Se<sup>2–</sup>, which is anticipated by the chemical analogy between the two chalcogenides. Herein, we report the first successful synthesis of Se-substituted bartonite, [Cs<sub>6</sub>Cl][Fe<sub>24</sub>Se<sub>26</sub>], a host–guest compound with a novel Fe–Se framework, together with investigations of its fundamental physical properties.

## Results

## Synthesis and chemical composition

The obtained polycrystalline sample and the small single crystals were black and elemental analyses (EDX) on ten crystallites from the powder sample gave an average composition of Cs<sub>6.3(4)</sub>Cl<sub>1.07(8)</sub>Fe<sub>25(1)</sub>Se<sub>25.1(6)</sub>. Within analytical errors, this result agrees well with the nominal composition and the results of the crystal structure determination.

## Structural analysis

The crystal structure of the title compound (Figure 1) consists of a host lattice built from octamers of fluorite-like edge-sharing FeSe<sub>4</sub> tetrahedra (Figure 2a–c), which form two crystallo-

[a] Dr. M. Valldor, Dr. B. Böhme, Dr. Yu. Prots, Dr. H. Borrmann, Dr. P. Adler, Dr. W. Schnelle, Dr. C. Y. Kuo, Dr. Z. Hu, Prof. Dr. C. Felser, Prof. Dr. L. H. Tjeng  
Max Planck Institute for Chemical Physics of Solids  
01187 Dresden (Germany)  
E-mail: martin.valldor@cpfs.mpg.de

[b] Dr. Y. Watier  
ESRF, 71 Avenue des Martyrs, 38000 Grenoble (France)

[c] Dr. T.-W. Pi  
National Synchrotron Radiation Research Centre, Hsinchu 30076 (Taiwan)

Supporting information for this article is available on the WWW under <http://dx.doi.org/10.1002/chem.201504840>.

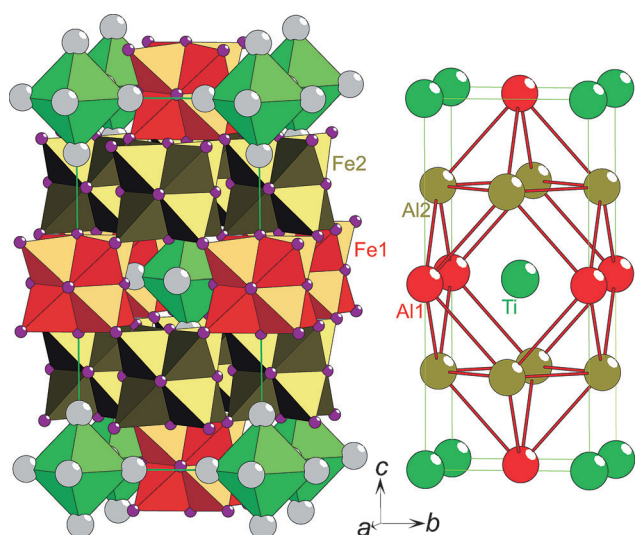


**Figure 1.** Left: The complete  $[\text{Cs}_6\text{Cl}][\text{Fe}_{24}\text{Se}_{26}]$  crystal structure, in which the  $[\text{Cs}_6\text{Cl}]^{5+}$  octahedra and the  ${}^3[\text{Fe}_8\text{Se}_6\text{Se}_{8/3}]$  units are highlighted. For better visualization, the latter (octamers) are shown in two colors to separate Fe1 (orange) and Fe2 (dark green). Right: The crystal structure of  $\text{TiAl}_3$ <sup>[16]</sup> is shown for comparison.

graphically distinct extended fused cubane  $[\text{Fe}_8\text{Se}_6\text{Se}_{8/3}]$  units. Each octamer of one type, Fe1(2), is connected to eight(four) octamers of the other type (Fe2(1)). Layers of each octamer are found perpendicular to the unique crystallographic axis. In a simplified description, half of the possible Fe1 octamers are replaced with  $[\text{Cs}_6\text{Cl}]$  octahedra (Figure 2d) in a checkerboard fashion, which is reversed in the neighboring layers to manifest the body centering (Figure 1). The structure can be described

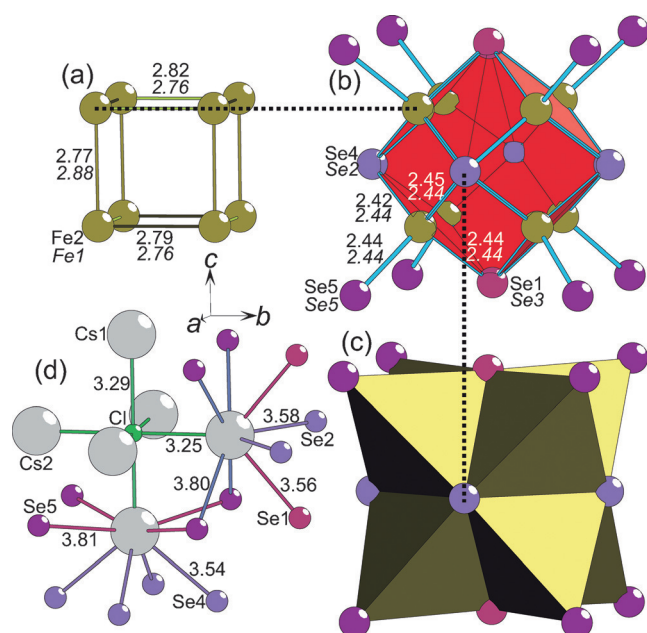


**Figure 2.** Crystal structure building blocks of  $[\text{Cs}_6\text{Cl}][\text{Fe}_{24}\text{Se}_{26}]$ . a)–c) The parts of an  $[\text{Fe}_8\text{Se}_6\text{Se}_{8/3}]$  extended fused cubane and d) the Se coordination around the  $[\text{Cs}_6\text{Cl}]^{5+}$  octahedra. Chosen interatomic distances [Å] are shown and the dashed lines are a guide for the eye between equivalent atoms.

on the basis of the nested polyhedra units approach<sup>[17]</sup> and regarded as a hierarchical derivate of the  $\text{TiAl}_3$ -type,<sup>[16]</sup> in which the  $[\text{Cs}_6\text{Cl}]$  units occupy the Ti and the  ${}^3[\text{Fe}_8\text{Se}_6\text{Se}_{8/3}]$  net occupies the Al positions. In turn, the  $\text{TiAl}_3$ -type constitutes a superstructure of *fcc* Cu<sup>[18]</sup> or a stuffed In-type crystal structure.<sup>[19]</sup>

From the expected charges of Cs, Cl, and Se and by assuming an ideal composition, a charge deficit on Fe is apparent. This can be balanced by 98% occupancy of the Fe sites in the host lattice; a similar situation is discussed for the closely related djerfisherite compound.<sup>[11]</sup> Alternatively, if all Fe sites are fully occupied, one delocalized electron could be distributed per three octamers. Or this charge deficit could also be accounted for if Cl was completely replaced with O that enters as an impurity in the solid-state reaction from the Fe metal. However, the expected Cs–O separation is about 2.86 Å, as taken from  $\text{Cs}_2\text{O}$ <sup>[20]</sup> and  $\text{Cs}_{11}[\text{Fe}_5\text{S}_8]_2\text{O}$ ,<sup>[21]</sup> in which O is octahedrally coordinated by Cs. Here the corresponding separation is 3.26 Å on average (Figure 2d). This is almost identical to the Cs–Cl separation in the host–guest compound  $[\text{Cs}_6\text{Cl}][\text{RE}_{21}\text{Ch}_{34}]$  ( $\text{RE} = \text{Dy, Ho, Ch} = \text{S, Se, Te}$ ) of 3.27 Å,<sup>[22]</sup> in which the charges add up properly with only  $\text{RE}^{+3}$ . Moreover, Cl was identified in fitting relative amounts, as estimated from EDX data. Thus, a minor iron deficiency in the title compound is the most probable explanation, but cannot be unambiguously resolved with the diffraction data at hand. As estimated by a synchrotron powder X-ray diffraction measurement (Figure S2 in the Supporting Information), the powder sample is relatively pure. Also, diffraction data obtained at 100 K suggest that the body-centered tetragonal symmetry persists even at relatively low temperatures.

### X-ray spectroscopy

The Fe- $L_{2,3}$  XAS spectrum of  $[\text{Cs}_6\text{Cl}][\text{Fe}_{24}\text{Se}_{26}]$  lies at the same energy as that of  $\text{Fe}^{2+}$  reference  $\text{Fe}_{0.04}\text{Mg}_{0.96}\text{O}$ ,<sup>[23]</sup> and is shifted by more than 1 eV to a lower energy with respect to  $\text{Fe}^{3+}$  reference  $\text{Fe}_2\text{O}_3$ , which demonstrates the  $\text{Fe}^{2+}$  valence state in  $[\text{Cs}_6\text{Cl}][\text{Fe}_{24}\text{Se}_{26}]$  (Figure 3). The similar multiplet spectral features of  $[\text{Cs}_6\text{Cl}][\text{Fe}_{24}\text{Se}_{26}]$  and  $\text{Fe}_{0.04}\text{Mg}_{0.96}\text{O}$  further indicates the same  $\text{Fe}^{2+}$  valence state, however, the features of the title compound are much broader. We ascribe this to the very strong Fe–Se covalence, not so much due to a large transfer integral but due to the relatively small Fe3d–Se4p charge-transfer energy, which makes these states practically degenerate. We note that the Fe–Se transfer integral is expected to be rather similar to that of Fe–O or Fe–S as a consequence of the larger Se atomic radius being compensated by the larger Fe–Se separation.

### Magnetism

The temperature-dependent magnetic susceptibility ( $\chi$ ) reveals that the title compound does not behave as a normal paramagnet even at 750 K, which indicates relatively strong spin–spin interactions (Figure 4). In the temperature range of 240 to 200 K, an anomaly in  $\chi$  is observed (Figure 4, upper right inset). In combination with data presented later, this suggests

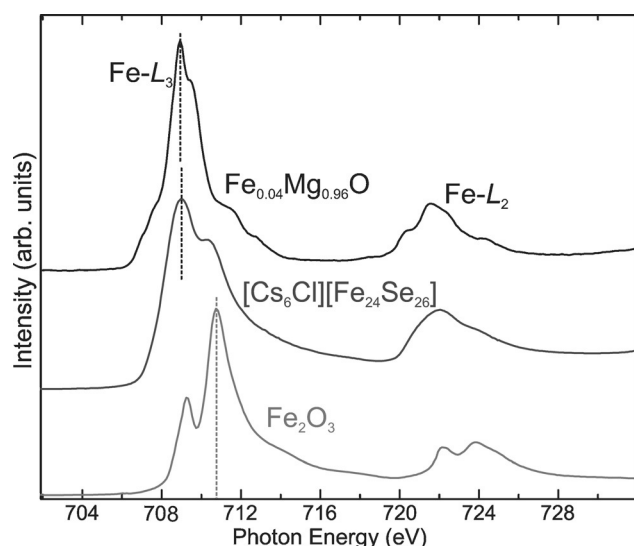


**Figure 3.** Fe- $L_{2,3}$  X-ray absorption spectroscopy (XAS) data of  $[\text{Cs}_6\text{Cl}][\text{Fe}_{24}\text{Se}_{26}]$  (middle),  $\text{Fe}_{0.04}\text{Mg}_{0.96}\text{O}$  (top, as  $\text{Fe}^{2+}$  reference), and  $\text{Fe}_2\text{O}_3$  (bottom, as  $\text{Fe}^{3+}$  reference). The dashed vertical lines represent the main intensity of each spectrum and are added as a guide for the eye.

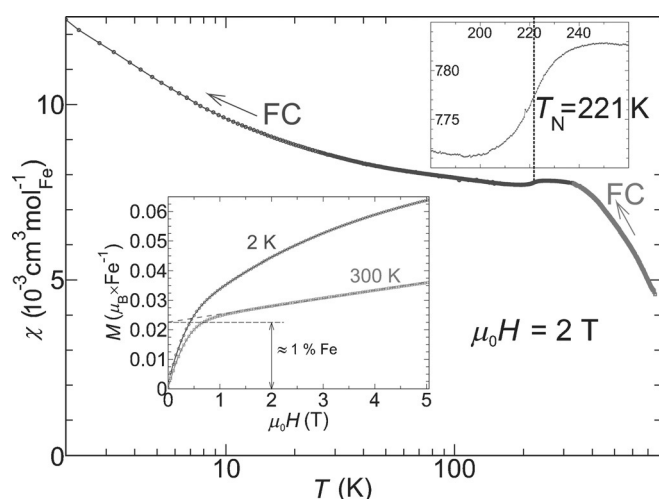


**Figure 4.** Magnetic susceptibility of  $[\text{Cs}_6\text{Cl}][\text{Fe}_{24}\text{Se}_{26}]$ . The temperature-dependent static-field magnetic susceptibility is shown. Upper inset: Magnification of data close to the  $T_N$ . Lower inset: Field-dependent magnetization data.

antiferromagnetic ordering with a Néel temperature ( $T_N$ ) of 221 K. The magnetization curve at 300 K indicates about 1% unreacted  $\alpha\text{-Fe}$ ,<sup>[24]</sup> which agrees with the Rietveld refinement. For comparison, the magnetism of the Bartonite sulfide mineral was only briefly mentioned as “weakly magnetic”,<sup>[12]</sup> but no data have been presented so far. Although the magnetic lattice of  $\text{BaFe}_2\text{Se}_3$  is very different (quasi-1D spin-ladders), the magnetic behavior is similar to that of the title compound, but with a  $T_N = 256$  K.<sup>[25]</sup> Thus, the magnetic  $\text{Fe}_4$  plaquettes that are suggested in  $\text{BaFe}_2\text{Se}_3$ <sup>[25]</sup> might be relevant in the title compound; the octamers could then be a combination of two pla-

quettes that are superimposed instead of being antiferromagnetically alternated along the ladders in  $\text{BaFe}_2\text{Se}_3$ .

### $^{57}\text{Fe}$ Mössbauer spectroscopy

The Mössbauer spectra of  $[\text{Cs}_6\text{Cl}][\text{Fe}_{24}\text{Se}_{26}]$  (Figure 5 and Figure S3 in the Supporting Information) reveal a single slightly

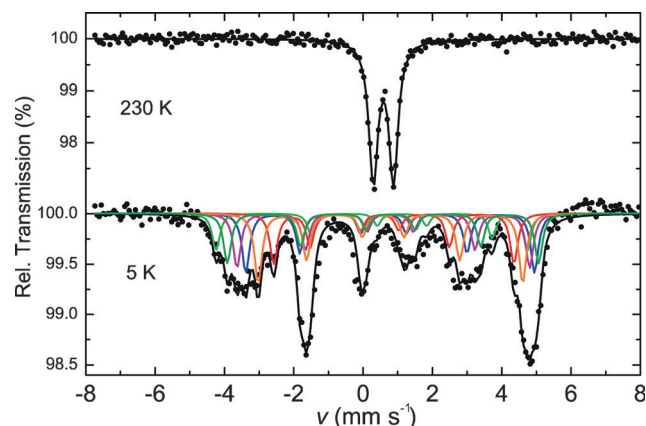


**Figure 5.** Mössbauer spectra of  $[\text{Cs}_6\text{Cl}][\text{Fe}_{24}\text{Se}_{26}]$  above and below  $T_N$ . The experimental data are plotted as dots, the calculated spectra are represented by black solid lines, and the colored lines correspond to the subspectra.

broadened quadrupole doublet for  $T > T_N$ , which indicates rapid spin–spin fluctuations ( $k > 10^8$  s $^{-1}$ ). The two iron sites ( $\text{Fe}1$ ,  $\text{Fe}2$ ) are very similar and not resolved. The isomer shifts ( $I_S$ ;  $0.55$  mm s $^{-1}$  at RT) are smaller than those for compounds with electronically localized  $\text{Fe}^{2+}$  ( $e^3t_2^3$ ), such as oxysulfides and oxyselenides ( $I_S \approx 0.68$  mm s $^{-1}$ ),<sup>[26]</sup> but larger than for electronically more itinerant compounds, such as semiconducting  $\text{BaFe}_2\text{S}_3$  ( $I_S = 0.41$  mm s $^{-1}$ )<sup>[27]</sup> or the metallic superconductor  $\beta\text{-FeSe}$  ( $I_S = 0.44$  mm s $^{-1}$ ).<sup>[2]</sup> This is in line with covalent Fe–Se bonding as suggested by the XAS results. Also, the quadrupole splitting ( $Q_S = 0.58$  mm s $^{-1}$ ) is smaller than expected for a localized  $e^3t_2^3$  configuration. The surprisingly complex magnetic hyperfine pattern at 5 K ( $T < T_N$ ) was simulated by a superposition of six sextets with equal  $I_S$  (see Section S3 in the Supporting Information for details and fit results). The sextets differ in their magnetic hyperfine fields ( $B_{\text{hf}}$ ) and quadrupole coupling parameters ( $Q_S$ ). The latter reflect the magnitude of the electric field gradient (efg) and the orientation between the efg and  $B_{\text{hf}}$ . The complex pattern may indicate a structural phase transition that involves tilts of  $\text{FeSe}_4$  tetrahedra, as suggested for  $\text{BaFe}_2\text{Se}_3$ ,<sup>[28]</sup> and/or a complex spin structure, such as that found in the spiral antiferromagnet  $\text{Sr}_2\text{FeO}_4$ .<sup>[29,30]</sup> Note that, because no obvious crystallographic changes were observed at 100 K (Figure S2 in the Supporting Information), the complex spin structure is more probable. Thus the magnetic ground state of the title compound might contain spin plaquettes, as suggested for  $\text{BaFe}_2\text{Se}_3$ ,<sup>[25]</sup> but with an additional ordering complexity.

## Resistivity measurements

The covalent bonding character of the Fe–Se host lattice agrees with the observed electric conductivity. At high temperatures, thermally activated conductivity behavior is observed with small activation energy (Figure 6). Below 221 K, the resi-

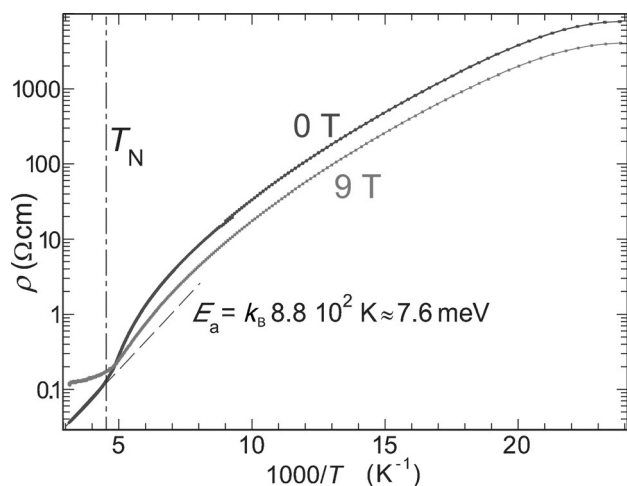


**Figure 6.** Electrical resistivity as a function of inverse temperature at two different magnetic fields. The Néel temperature is indicated by a vertical broken line and an Arrhenius estimation of the activation energy (dashed line) has been fitted to the high-temperature data at 0 T.

tivity ( $\rho$ ) increases as expected for a lattice with antiferromagnetic spin ordering. Due to strong exchange interactions in the title compound, a magnetic field has a relatively weak influence on the conducting electrons, but it increases  $\rho$  above  $T_N$ , whereas it decreases  $\rho$  below  $T_N$ . Thus, a considerable magneto-resistance is observed. The estimated thermal activation energy gap of 7.6 meV represents a minimum, which is possibly influenced by impurity states. The fundamental thermal activation energy might be larger.

## Specific heat capacity

In the temperature range of 170 to 250 K, the specific heat data exhibit an anomaly with a maximum close to 221 K (Figure 7). The asymmetry and broadness of this anomaly indicate a second-order phase transition, which confirms the magnetic ordering of the title compound. However, close to 221 K the released spin entropy per iron spin (Figure 7, inset) is  $36.7 \text{ J mol}^{-1} \text{ K}^{-1} / 24 = 1.53 \text{ J mol}^{-1} \text{ K}^{-1}$ , which is far from the expected  $R \ln(2J + 1) = 13.4 \text{ J mol}^{-1} \text{ K}^{-1}$  for  $J = 2$ . Possibly the entropy is released within a larger temperature range than presumed in this simple estimation.

## Discussion

Although the bartonite mineral was suggested to form in aqueous solution under hydrothermal conditions,<sup>[10]</sup> the isostructural title compound was synthesized from binary precursors and elements. The success of this route ensures relatively

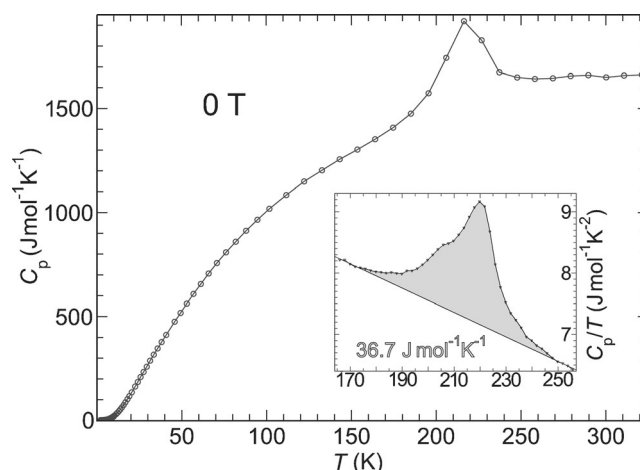


**Figure 7.** Specific heat capacity of  $[\text{Cs}_6\text{Cl}][\text{Fe}_{24}\text{Se}_{26}]$ . Inset: The integrated area of the  $C_p/T(T)$  plot that was used to obtain the magnetic ordering entropy.

easy access to novel compounds with novel Fe–Se lattices, as presented herein.

The building block  $[\text{Fe}_8\text{Se}_6\text{Se}_{8/3}]$  is a chemical extension of the known fused cubanes that can be found as complex ions  $[\text{Fe}_8\text{S}_6\text{I}_8]^{4-}$ , in which eight iodine atoms sit at the terminating corner sites.<sup>[15]</sup>  $\text{Fe}_8\text{S}_6$  is further found in, for example, djerfisherite,<sup>[11]</sup> pentlandite,<sup>[12]</sup>  $[\text{Fe}_8\text{S}_6\text{Cl}_4(\text{PCy}_3)_4] \cdot 3 \text{ THF}$ ,<sup>[31]</sup> ( $\text{PCy}_3$  = tricyclohexylphosphine, THF = tetrahydrofuran), and  $(\text{PPN})_2[\text{Fe}_8\text{S}_6(\text{NO})_8]$  (PPN = bis(triphenylphosphine)iminium),<sup>[32]</sup> which emphasizes its commonness. All cubane-like compounds are of great interest with respect to catalytic activity in the natural enzyme nitrogenase.<sup>[13–15]</sup> The title compound proves that Se-based fused cubane is obtainable, which opens up prospects to alter the catalytic activity of Fe cubane and related cluster centers.

The strongly ionic guest  $[\text{A}_6\text{Cl}]^{5+}$  ( $\text{A} = \text{Cs}, \text{K}$ ) occurs within strongly covalent host lattices in at least three well-characterized compounds: bartonite,<sup>[9,10]</sup> djerfisherite,<sup>[11]</sup> and  $[\text{Cs}_6\text{Cl}][\text{RE}_{21}\text{Ch}_{34}]$  ( $\text{RE} = \text{Dy}, \text{Ho}, \text{Ch} = \text{S}, \text{Se}, \text{Te}$ ).<sup>[21]</sup> By comparing bartonite with  $[\text{Cs}_6\text{Cl}][\text{RE}_{21}\text{Ch}_{34}]$ , it is evident that the resulting charge of the host lattice is important for the overall periodicity of the  $[\text{A}_6\text{Cl}]^{5+}$  ion. The higher the charge of the chalcogenide-based host, the shorter the distance between the guest ions, as expected.

The crystal structure of the title compound, except for the part replaced with the guest ion, is a cubic close-packed Se lattice with  $\text{Fe}^{2+}$  solely in the tetrahedral voids, which emphasizes its close structural relationship to the superconductor  $\text{Fe}_{1+x}\text{Se}$ . The main difference is the distribution of  $\text{Fe}^{2+}$  ions: The title compound has  $\text{Fe}^{2+}$  ions in eight neighboring tetrahedral voids surrounded by a “shell” of unoccupied tetrahedral voids, whereas  $\text{Fe}_{1+x}\text{Se}$  has  $\text{Fe}^{2+}$  in all tetrahedral voids within layers that are separated by layers of empty tetrahedra.<sup>[1]</sup> Nevertheless, the Fe–Se separations in the title compounds (Figure 2b) are remarkably similar to those in  $\text{Fe}_{1+x}\text{Se}$  (2.39 Å).<sup>[2]</sup> Also, the Fe–Fe separations of about 2.76 to 2.88 Å in the octamers are not far from those found in  $\text{Fe}_{1+x}\text{Se}$  (2.67 Å),<sup>[2]</sup>

$\text{K}_{0.8}\text{Fe}_2\text{Se}_2$  (2.77 Å),<sup>[33]</sup> and Fe pnictides that show superconductivity.

Evidently,  $[\text{Cs}_6\text{Cl}][\text{Fe}_{24}\text{Se}_{26}]$  is an antiferromagnetic insulator and not a superconductor. Yet we can infer that the compound is very close to being a conductor; its bandgap must be rather small. Although the activation energy, as deduced from the resistivity measurements, may not be a reliable indicator, data from other measurements do provide strong hints: 1) the broad XAS features suggest that the Fe3d and Se4p orbitals are degenerate in energy, which facilitates the hopping of charge carriers, 2) the Mössbauer parameters refute a well-localized  $e^3t_2^3$  electronic configuration, and 3) the high Néel temperature together with the absence of a Curie–Weiss behavior up to 750 K imply relatively strong exchange or super-exchange interactions and, therefore, rather low virtual excitation energies. Therefore, we expect that pressure, a decrease in the Fe–Fe separation, or doping can easily bring the title compound into itinerancy with suppressed magnetism and perhaps even superconductivity.

## Conclusion

The host–guest compound  $[\text{Cs}_6\text{Cl}][\text{Fe}_{24}\text{Se}_{26}]$  can be obtained through solid-state reactions in closed vessels. The Fe–Se lattice is built from edge-sharing fused-cubane entities  $[\text{Fe}_8\text{Se}_6\text{Se}_{8/3}]$ , in which the divalent, tetrahedrally coordinated Fe is found as octamers. An antiferromagnetic state is observed below  $T_N = 221$  K and the complex Mössbauer spectra suggest a non-trivial magnetic ground state. The strong covalent bonding based on a near degeneracy of the Fe3d and Se4p orbitals together with small energies for virtual excitations indicate that the title compound is close to electronic itinerancy.

## Experimental Section

### Sample preparation

The  $\text{Cs}_2\text{Se}$  precursor was synthesized by reacting Cs metal (3 N, Chempur) with elemental Se (5 N, Alfa). Cs metal was placed in a Ta tube with one end open. The corresponding stoichiometric amount of Se was placed in a smaller Ta tube that fit into the first one. Care was taken to not let the tube fall over. Subsequently, the outer Ta tube was weld-sealed. The sample was heated for 12 h at 210 °C, then heated at a rate of 50 °C h<sup>-1</sup> to 800 °C, and finally cooled to RT at the same rate.  $\text{Cs}_2\text{Se}$  was bright grey on grinding.

Stoichiometric amounts of powdered  $\text{Cs}_2\text{Se}$ , CsCl (3 N, TRC), Fe (3 N, Alfa), and Se (2.5:1:24:23.5) were mixed in an agate mortar in a controlled atmosphere ( $\text{O}_2$  and  $\text{H}_2\text{O} < 0.1$  ppm, MBraun Labmaster glove box). Pellets of the mixture were reacted in corundum crucibles inside evacuated ( $< 10^{-7}$  bar) silica tubes. The sample was annealed for 60 h at 500 °C with slow heating and cooling. Without exposure to air, the sample was reground, repelletized, and heated again in the same way to afford the compound powder investigated herein.

Small single crystals were grown in CsCl flux inside an evacuated silica ampoule. A mixture with a Fe/Se/SeO<sub>2</sub>/CsCl molar ratio of 4:1:1:3 was heated to 750 °C within 6 h. Subsequently the mixture was held at this temperature for 96 h, then cooled to 500 °C over

96 h, before the furnace was switched off. The well-shaped crystals were mechanically separated from the CsCl residue and were stable in air for several days.

### X-ray diffraction

Single-crystal data were obtained by using a Rigaku AFC7 with a CCD camera as the detector (Saturn 724+), and a  $\text{Mo}_{K\alpha}$  X-ray source ( $\lambda = 0.71073$  Å). The empirically absorption-corrected data (multi-scan) were further treated by using JANA2006.<sup>[34]</sup> A structural model was found by using charge flipping in Superflip. In the final refinement, all atomic positions were refined as fully occupied and with harmonic anisotropic displacement parameters. Details can be found in the Supporting Information (Section S1).

Powder X-ray data were obtained at the high-resolution powder diffraction beamline ID22 (ESRF, Grenoble) by using a constant wavelength of  $\lambda = 0.400737(6)$  Å and a 0.3 mm glass capillary as the sample holder, Debye–Sherrer mode, and a nine-crystal multianalyzer as the detector. The Rietveld refinement was completed by using JANA2006.<sup>[34]</sup>

### Elemental analysis

A scanning electron microscope (SEM XL30) equipped with an energy-dispersive X-ray spectrometer (EDX) from Philips, working at 25 kV, was used for elemental analysis. The sample was briefly exposed to air during the transport into the microscope, but there was no obvious sample degradation.

### Spectroscopy

Soft X-ray absorption spectroscopy (XAS) at the Fe- $L_{2,3}$  edge was measured at the BL08B beamline of the National Synchrotron Radiation Research Centre (NSRRC) in Taiwan. The Fe- $L_{2,3}$  XAS spectra of  $[\text{Cs}_6\text{Cl}][\text{Fe}_{24}\text{Se}_{26}]$  together with  $\text{Fe}_{0.04}\text{Mg}_{0.96}\text{O}^{[23]}$  and  $\text{Fe}_2\text{O}_3$  as  $\text{Fe}^{2+}$  and  $\text{Fe}^{3+}$  references, respectively, were taken in the total electron yield (TEY) mode with a photon energy resolution of 0.2 eV. Clean sample surfaces were obtained by cutting pellets in situ just before collecting the data in an ultrahigh vacuum chamber with the pressure in the mid- $10^{-10}$  mbar range.

Mössbauer spectra were collected by using a standard WissEl spectrometer operated in the constant acceleration mode and with a <sup>57</sup>Co/Rh source. A powder sample was mixed with BN and placed in a Plexiglas container. The Fe content was  $\approx 10$  mg cm<sup>-2</sup>. Spectra between 4.7 and 290 K were obtained by using a Janis-SHI-850–5 closed cycle refrigerator (CCR). The isomer shifts are given relative to  $\alpha$ -Fe. The data were evaluated by using the program MossWinn<sup>[35]</sup> and the thin absorber approximation.

### Physical properties

Magnetization data were obtained by using a MPMS-XL instrument (Quantum Design). In the range of 2–350 K, a polycarbonate capsule was used as sample holder, and between 300 and 750 K, a high-purity silica tube was used. Temperature-dependent data were obtained at a constant field of 2 T and the high-temperature data were shifted to account for the temperature-independent signal from the furnace.

A standard four-point method was used, in which the application of ac or dc current delivered temperature-dependent resistivity data by using a physical property measurement system (PPMS, Quantum Design). Gold contacts were fastened to a polycrystalline piece with silver-filled epoxy inside a glovebox. The setup was

quickly transferred to the cryostat with exposure to air for only a few seconds.

To extract the specific heat, the nonadiabatic thermal relaxation method of the HC option setup of the PPMS (Quantum Design) was used. A well-sintered sample piece was attached to the holder by using Apiezon N grease. Due to the air sensitivity of the sample, the mounting was performed in a glovebox and the sample was protected by a thin layer of grease during the short exposure to air between box and cryostat.

## Acknowledgements

We thank Rüdiger Kniep, Daniel Khomskii, and Deepa Kasinathan for their invaluable comments. Ralf Koban is acknowledged for assistance with the thermodynamic measurements. We also thank Petra Scheppan for the electron microscopy studies (EDX).

**Keywords:** inorganic synthesis · iron · magnetic properties · Mössbauer spectroscopy · X-ray diffraction

- [1] F. C. Hsu, J. Y. Luo, K. W. Yeh, T. K. Chen, T. W. Huang, P. M. Wu, Y. C. Lee, Y. L. Huang, Y. Y. Chu, D. C. Yan, M. K. Wu, *Proc. Natl. Acad. Sci. USA* **2008**, *105*, 14262–14264.
- [2] T. M. McQueen, A. J. Williams, P. W. Stephens, J. Tao, Y. Zhu, V. Ksenofontov, F. Casper, C. Felser, R. J. Cava, *Phys. Rev. Lett.* **2009**, *103*, 057002.
- [3] S. Tan, Y. Zhang, M. Xia, Z. Ye, F. Chen, X. Xie, R. Peng, D. Xu, Q. Fan, H. Xu, J. Jiang, T. Zhang, X. Lai, T. Xiang, J. Hu, B. Xie, D. Feng, *Nat. Mater.* **2013**, *12*, 634–640.
- [4] M. Burrard-Lucas, D. G. Free, S. J. Sedlmaier, J. D. Wright, S. J. Cassidy, Y. Hara, A. J. Corkett, T. Lancaster, P. J. Baker, S. J. Blundell, S. J. Clarke, *Nat. Mater.* **2013**, *12*, 15–19.
- [5] T. P. Ying, X. L. Chen, G. Wang, S. F. Jin, T. T. Zhou, X. F. Lai, H. Zhang, W. Y. Wang, *Sci. Rep.* **2012**, *2*, 426.
- [6] Y. Peng, G. Xi, C. Zhong, L. Wang, J. Lu, X. Sun, L. Zhu, Q. Han, L. Chen, L. Shi, M. Sun, Q. Li, M. Yu, M. Yin, *Geochim. Cosmochim. Acta* **2009**, *73*, 4862–4878.
- [7] G. K. Czamanske, M. A. Lanphere, R. C. Erd, M. C. Blake Jr., *Earth Planetary Sci. Lett.* **1978**, *40*, 107–110.
- [8] G. K. Czamanske, R. C. Erd, B. F. Leonard, J. R. Clark, *Am. Mineral.* **1981**, *66*, 369–375.
- [9] H. T. Evans Jr., J. R. Clark, *Am. Mineral.* **1981**, *66*, 376–384.
- [10] V. N. Yakovenchuk, Y. A. Pakhomovsky, Yu. P. Men'shikov, G. Yu. Ivanyuk, S. V. Krivovichev, P. C. Burns, *Can. Mineral.* **2003**, *41*, 503–511.
- [11] B. S. Tani, *Am. Mineral.* **1977**, *62*, 819–823.
- [12] M. Lindqvist, D. Lindqvist, A. Westgren, *Sv. Kem. Tids.* **1936**, *48*, 156–160.
- [13] J. Kim, D. C. Rees, *Science* **1992**, *257*, 1677–1682.
- [14] J. Kim, D. C. Rees, *Nature* **1992**, *360*, 553–560.
- [15] S. Pohl, U. Opitz, *Angew. Chem. Int. Ed. Engl.* **1993**, *32*, 863–864; *Angew. Chem.* **1993**, *105*, 950–952.
- [16] G. Brauer, *Z. Anorg. Allg. Chem.* **1939**, *242*, 1–22.
- [17] B. Chabot, K. Cenzual, E. Parthé, *Acta Crystallogr. Sect. A* **1981**, *37*, 6–11.
- [18] W. L. Bragg, *Philos. Mag.* **1914**, *28*, 255–360.
- [19] A. W. Hull, W. P. Davey, *Phys. Rev.* **1921**, *17*, 266–267.
- [20] A. Helms, W. Klemm, *Z. Anorg. Allg. Chem.* **1939**, *242*, 33–40.
- [21] M. Schwarz, C. Röhr, *Z. Anorg. Allg. Chem.* **2014**, *640*, 2792–2800.
- [22] H. Lin, L. H. Li, L. Chen, *Inorg. Chem.* **2012**, *51*, 4588–4596.
- [23] T. Haupricht, R. Sutarto, M. W. Haverkort, H. Ott, A. Tanaka, H. H. Hsieh, H. J. Lin, C. T. Chen, Z. Hu, L. H. Tjeng, *Phys. Rev. B* **2010**, *82*, 035120.
- [24] C. Koz, M. Schmidt, H. Borrmann, U. Burkhardt, S. Rößler, W. Carrillo-Cabrera, W. Schnelle, U. Schwarz, Yu. Grin, *Z. Anorg. Allg. Chem.* **2014**, *640*, 1600–1609.
- [25] J. M. Caron, J. R. Neilson, D. C. Miller, A. Llobet, T. M. McQueen, *Phys. Rev. B* **2011**, *84*, 180409.
- [26] M. Valldor, P. Adler, Yu. Prots, U. Burkhardt, L. H. Tjeng, *Eur. J. Inorg. Chem.* **2014**, *36*, 6150–6155.
- [27] W. M. Reiff, I. E. Grey, A. Fan, Z. Eliezer, H. Steinfink, *J. Solid State Chem.* **1975**, *13*, 32–40.
- [28] K. Komędera, A. K. Jasek, A. Błachowski, K. Ruebenbauer, M. Piskorz, J. Żukrowski, A. Krztoń-Maziopa, E. Pomjakushina, K. Conder, *Solid State Commun.* **2015**, *207*, 5–8.
- [29] S. E. Dann, M. T. Weller, D. B. Currie, M. F. Thomas, A. D. Al-Rawwas, *J. Mater. Chem.* **1993**, *3*, 1231–1237.
- [30] P. Adler, *J. Solid State Chem.* **1994**, *108*, 275–283.
- [31] C. Goh, B. M. Segal, J. Huang, J. R. Long, R. H. Holm, *J. Am. Chem. Soc.* **1996**, *118*, 11844–11853.
- [32] H. Kalyvas, D. Coucouvanis, *Inorg. Chem.* **2006**, *45*, 8462–8464.
- [33] J. Guo, S. Jin, G. Wang, S. Wang, K. Zhu, T. Zhou, M. He, X. Chen, *Phys. Rev. B* **2010**, *82*, 180520.
- [34] V. Petříček, M. Dušek, L. Palatinus, JANA2006, Institute of Physics, Academy of Sciences of the Czech Republic, Praha (Czech Republic), **2013**.
- [35] <http://moss Winn.com>.

Received: December 2, 2015

Published online on February 16, 2016